








Reduction of photodynamic damage of blood vessels in the protected region by (-)-epigallocatechin gallate

Tianlong Chen ^{*}, Yi Shen ^{*,†,**,¶}, Li Lin ^{*}, Huiyun Lin ^{*},
Xuejiao Song [†], Defu Chen [‡] and Buhong Li ^{*,§,||,***}

^{*}*MOE Key Laboratory of OptoElectronic Science and Technology for Medicine
Fujian Provincial Key Laboratory of Photonics Technology, Fujian Normal University
Fuzhou 350117, P. R. China*

[†]*Key Laboratory of Flexible Electronics and Institute of Advanced Materials
Nanjing Technology University, Nanjing 211800, P. R. China*

[‡]*School of Medical Technology, Beijing Institute of Technology
Beijing 100081, P. R. China*

[§]*School of Physics and OptoElectronic Engineering, Hainan University
Haikou 570228, P. R. China*

[¶]*yishen@fjnu.edu.cn*

^{||}*bhli@hainanu.edu.cn*

Received 1 October 2023

Revised 12 January 2024

Accepted 14 January 2024

Published 9 March 2024

Photodynamic therapy (PDT) has been increasingly used in the clinical treatment of neoplastic, inflammatory and infectious skin diseases. However, the generation of reactive oxygen species (ROS) may induce undesired side effects in normal tissue surrounding the treatment lesion, which is a big challenge for the clinical application of PDT. To date, (-)-Epigallocatechin gallate (EGCG) has been widely proposed as an antiangiogenic and antitumor agent for the protection of normal tissue from ROS-mediated oxidative damage. This study evaluates the regulation ability of EGCG for photodynamic damage of blood vessels during hematoporphyrin monomethyl ether (Hemoporphin)-mediated PDT. The quenching rate constants of EGCG for the triplet-state Hemoporphin and photosensitized ¹O₂ generation are determined to be $6.8 \times 10^8 \text{ M}^{-1}\text{S}^{-1}$ and $1.5 \times 10^8 \text{ M}^{-1}\text{S}^{-1}$, respectively. The vasoconstriction of blood vessels in the protected region treated with EGCG hydrogel after PDT is lower than that of the control region treated with pure hydrogel, suggesting an efficiently reduced photodamage of Hemoporphin for blood vessels treated with EGCG. This study indicates that EGCG is an efficient quencher for triplet-state Hemoporphin and ¹O₂, and EGCG could be potentially used to reduce the undesired photodamage of normal tissue in clinical PDT.

Keywords: (-)-Epigallocatechin gallate (EGCG); photodynamic therapy; hemoporphin; singlet oxygen; blood vessel; vasoconstriction.

**Corresponding authors.

1. Introduction

Photodynamic therapy (PDT) has been widely regarded as a safe and effective therapeutic method for malignant and benign skin diseases. An ideal PDT process is expected to completely eradicate lesions while preserving the functionally important structures of surrounding normal tissue. However, the generation of reactive oxygen species (ROS) during PDT, particularly singlet oxygen ($^1\text{O}_2$) in the surrounding normal tissue may induce early or late-onset side effects, which include erythema, burns, edema and itching.¹ An effective strategy to address this issue is to develop the third-generation photosensitizer (PS) with difference targeting agents.²⁻⁴ Nevertheless, the clinically approved PSs, such as Foscan, Visudyne and Hematoporphyrin monomethyl ether (Hemoporphin), do not have the targeted ability for specific subcellular localization. Therefore, taking advantage of natural antioxidants as a $^1\text{O}_2$ quencher could be an important strategy to prevent surrounding normal tissue from undesired damages.

As a well-known natural antioxidant, (-)-Epigallocatechin gallate (EGCG) possesses versatile biological functions, including free radical scavenging ability, regulation of gene expression and molecular signaling pathways.⁵⁻⁸ Specifically, the regulatory function of EGCG to quench the ROS during photosensitization, has been intensively investigated.⁹⁻¹² Choi *et al.* studied the impact of EGCG structure on $^1\text{O}_2$ quenching activity in methanol. The quenching rate of EGCG for $^1\text{O}_2$ was determined to be $1.31 \times 10^8 \text{ M}^{-1}\text{s}^{-1}$, which was further demonstrated to be affected by the pyrogallol ring structure of EGCG.¹³ Okazaki *et al.* reported that EGCG and α -Tocopherol could significantly scavenge $\cdot\text{OH}$ and $^1\text{O}_2$, and EGCG appear to be more efficient to quench O_2^- and H_2O_2 than α -Tocopherol.¹⁴ In another study, we evaluated the quenching effects of different natural antioxidants including EGCG, Procyanidins, L-carnosine and Vitamin C in air-saturated phosphate buffered saline (PBS) during photosensitization.¹⁵ The obtained results indicated that EGCG possessed the strongest quenching ability as compared to the others, and a significantly reduced oxidative damage for NIH/3T3 cells was observed after Ce6-mediated PDT. Most recently, based on the self-assembly of methyl-pheophorbide, a derivative MPa-TEG (MT), and EGCG, Yang *et al.*

constructed a J-aggregated nano-porphyrin which is termed as MTE, showing that MTE could effectively avoid undesired side effects of phototoxicity due to the scavenging ability of ROS.¹⁶ Although fruitful achievements had been reported, the actual role and fundamental mechanisms of EGCG against photodynamic damage are not fully clarified yet.

In this study, the regulation ability of EGCG, which reduces the photodynamic damage of blood vessels in the dorsal skinfold window chamber (DSWC) of ICR mice after PDT, was quantitatively evaluated. For the PDT treatment, Hemoporphin, a clinically approved PS for port wine stain treatment in P. R. China, was employed as a PS model. First, the quenching effects of EGCG for $^1\text{O}_2$ during photosensitization were investigated through the analysis of absorption, fluorescence and time-resolved $^1\text{O}_2$ luminescence spectra of Hemoporphin in air-saturated PBS at 1270 nm. In addition, a self-built multi-modal imaging system was utilized to simultaneously monitor the fluorescence intensity of Hemoporphin, blood flow velocity, as well as vasoconstriction (i.e., reduction in vascular diameter) of blood vessels during EGCG-involved and Hemoporphin-mediated PDT. Furthermore, EGCG hydrogel was prepared and topically administered on blood vessels in the DSWC model before PDT to evaluate the regulation ability of EGCG.

2. Materials and Methods

2.1. Chemicals

Hemoporphin[®] was purchased from Shanghai Fudan-Zhangjiang Bio-Pharmaceutical Co., Ltd. (Shanghai, China). EGCG and calcium chloride (CaCl_2) were obtained from Sigma-Aldrich (St. Louis, MO, USA). Sodium alginate and agar powder were provided by Beijing Solarbio Science & Technology Co., Ltd. (Beijing, China). Hemoporphin stock solution of 100 mg/kg was prepared using air-saturation sterilized saline and stored at 4°C in darkness, followed by dilution of Hemoporphin stock solution to 3.75 mg/mL before use.

2.2. Absorption and fluorescence spectra measurement

The UV/Vis/NIR spectrophotometer (Lambda 950, Perkin Elmer, Waltham, MA, USA) and spectrofluorometer (FLS920, Edinburgh Instruments Ltd.,

Livingston, UK) were utilized to measure the absorption and fluorescence spectra of Hemoporphin, EGCG and the mixture of Hemoporphin and EGCG in PBS (pH = 7.2) at room temperature, respectively. For all measurements, samples were placed in a standard 10 mm path length quartz cuvette (101-QS, Hellma, Müllheim, GER).

2.3. Time-resolved¹ O₂ luminescence measurement

The time-resolved ¹O₂ luminescence spectra were obtained using a highly sensitive detection system, which has been previously described.^{15,17} In order to excite Hemoporphin, a 523 nm diode-pumped, Q-switched, frequency-doubled Nd: YLF laser (QG-523-500, CrystaLaser Inc.) with a pulse width of 25 ns was used as the excitation source. All spectral data were processed and graphed using Origin Pro 8.5 (OriginLab Corp.), and the integrated ¹O₂ luminescence intensity I at 1270 nm was calculated according to Eq. (1).^{17,18}

$$I = (I_{1270}^S - I_{1270}^C) - \frac{(I_{1230}^S - I_{1230}^C) + (I_{1310}^S - I_{1310}^C)}{2}, \quad (1)$$

where I_{1270}^S , I_{1230}^S and I_{1310}^S represent the integrated intensity of Hemoporphin in the absence and presence of EGCG at 1270, 1230 and 1310 nm, and I_{1270}^C , I_{1230}^C and I_{1310}^C stand for the integrated intensity of the control group.

Furthermore, the lifetimes of triplet state Hemoporphin (τ_T) and ¹O₂ (τ_Δ) were obtained by fitting the time-resolved ¹O₂ luminescence decay curves using Eq. (2).^{17,18}

$$I(t) = A \frac{\tau_\Delta}{\tau_\Delta - \tau_T} [\exp(-t/\tau_\Delta) - \exp(-t/\tau_T)] + I_0, \quad (2)$$

where $I(t)$ denotes the time-dependent photon counts captured by the near-infrared photon multiplier tube (PMT), and the amplitude parameter and offset derived from the PMT noise were defined as A and I_0 , respectively.

2.4. Preparation of EGCG hydrogel

Initially, 1.5 wt.% sodium alginate solution was prepared by dissolving 1.5 g solidium alginate in 100 mL of deionized water at 40°C. The prepared

solution was sterilized by filtration through 220 nm filter and stored in 4°C before processing. 1.1 wt.% CaCl₂ solution containing 1.1 wt.% agar powder after autoclave sterilization was prepared and poured into 6-well petri culture dishes to form pre-gel solution. Afterward, various concentrations of EGCG (0, 10, 20, 30 mg/mL) were prepared by dispersing 0, 4, 8 and 12 mg of EGCG into 400 μ L of 1.5 wt.% sodium alginate solution. By incorporating the EGCG solution into the pre-gel solution, hydrogel alone or hydrogel with EGCG was formed after cross-linking reaction between Ca(II) and sodium alginate for 0.5 h.^{18,19} The time needed for cross-linking was verified by tilting petri culture dishes until the flow of solution was unobservable.

2.5. Blood vessels in DSWC model for PDT

A total of 30 ICR male mice (25–30 g) used in this study were obtained from Shanghai SLAC Experimental Animals Co., LTD. For visualizing the blood vessels, a pair of titanium frames (APJ Trading Co., Ventura, CA, USA) was surgically implanted on both sides of DSWC based on a well-established protocol.²⁰ 21 ICR mice were randomly assigned into seven groups ($n = 3$), with groups of 2–7 used for verifying the antioxidation effects of EGCG solution *in vivo*. Considering the potential instability of EGCG molecules,²¹ the 0.2 mL mixed agents consisting of 3.75 mg/mL Hemoporphin and various EGCG concentrations were injected into the tail vein of mice immediately after being prepared with sterilized saline. For PDT studies, the administered dose of Hemoporphin is 25 mg/kg b.w. for each ICR mouse, while the doses for EGCG ranged from 0 to 80 mg/kg b.w., as listed in Table 1. For the Hemoporphin-mediated PDT, the blood vessels of the DSWC model were uniformly irradiated by the 532 nm semiconductor laser 1.0 min after administration of the mixed agent. The power density of irradiation was 50 mW/cm² and the total light dose for each PDT treatment was 22.5 J/cm².

In addition, the other 9 ICR mice were randomly assigned into three groups ($n = 3$) to confirm the potential of EGCG hydrogel in the application of healthy tissue protection during PDT. To achieve this purpose, hydrogels with various EGCG concentrations were prepared, as shown in Table 2.

Table 1. Various EGCG concentrations for Hemoporfin-mediated PDT *in vivo*.

Group	Drug delivery	Hemoporfin concentration (mg/kg b.w.)	EGCG concentration (mg/kg b.w.)
1	EGCG	0	80
2	Hemoporfin	25	0
3	Hemoporfin + EGCG	25	10
4	Hemoporfin + EGCG	25	20
5	Hemoporfin + EGCG	25	40
6	Hemoporfin + EGCG	25	60
7	Hemoporfin + EGCG	25	80

Table 2. Hydrogel with various EGCG concentrations for Hemoporfin-mediated PDT *in vivo*.

Group	Drug delivery	EGCG concentration (mg/mL)
1	Hemoporfin + pure hydrogel	0
	Hemoporfin + EGCG hydrogel	10
2	Hemoporfin + pure hydrogel	0
	Hemoporfin + EGCG hydrogel	20
3	Hemoporfin + pure hydrogel	0
	Hemoporfin + EGCG hydrogel	30

Two kinds of hydrogels in the absence and presence of EGCG were simultaneously applied topically on blood vessels in the DSWC model for 1.0 h, as presented in Fig. 1, prior to the Hemoporfin injection through tail veins of the ICR mice. In the application process of hydrogel, the interval between the glass window and the titanium frame was sealed with an adhesive bandage to minimize the oxidation of EGCG. During PDT, the mouse was anesthetized and ventilated with 2% isoflurane mixed in oxygen, and the O₂ flow meter was set to 1.0 L/min. All protocols in this study were approved by the Institutional Animal Care and Use Committee of the Fujian Normal University, and the

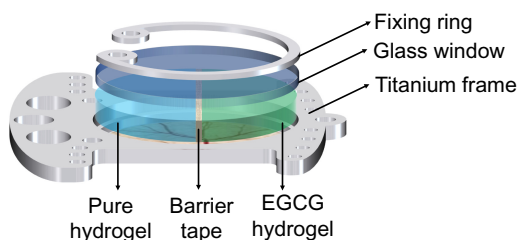


Fig. 1. Schematic diagram of hydrogel in absence and presence of EGCG applied in DSWC model for PDT.

ICR mice were treated in accordance with the NIH Guide for the Care and Use of Laboratory Animals.

2.6. Image processing and data analysis

Images of blood vessels in the DSWC model were captured using a self-built multi-modal system which consists of narrow band imaging (NBI), fluorescence imaging (FI) and laser speckle contrast imaging (LSCI).²² The captured multi-modal images were processed by MATLAB-based custom algorithm which first executed an area extraction of artery and vein mainly based on NBI, followed by image registration between FI and LSCI.^{23,24} Afterwards, fluorescence intensity of Hemoporfin, relative blood flow velocity and vasoconstriction of blood vessels were quantified for analysis, respectively. Among these, the vasoconstriction V was defined as in Eq. (3):¹⁸

$$V = \left(1 - \frac{D_t}{D_o}\right) \times 100\%, \quad (3)$$

where D_0 and D_t represent the targeted vascular area before and after Hemoporfin-mediated PDT, respectively.

3. Results

3.1. Absorption and fluorescence spectra of EGCG

As shown in Fig. 2(a), the absorption spectrum of Hemoporfin in air-saturated PBS has a maximal absorbance peaking at 391 nm. The absorption spectrum is nearly unchanged for the mixture of Hemoporfin+EGCG in PBS, suggesting no chemical reaction between EGCG and Hemoporfin. As presented in Fig. 2(b), the red fluorescence peaks of Hemoporfin located at 612 nm and 674 nm, while no apparent EGCG fluorescence was detected in the spectral region from 560 nm to 750 nm. As compared to the pure Hemoporfin, the fluorescence intensity peaks of the Hemoporfin added with EGCG of various concentrations (0.1, 0.4, 0.8 mM) in PBS were decreased by 13.85% and 12.97%, respectively.

3.2. Quenching rate constant of EGCG for photosensitized ¹O₂ generation

The quenching ability of EGCG was evaluated for Hemoporfin-mediated photosensitized ¹O₂ generation. As shown in Fig. 3(a), the time-resolved ¹O₂

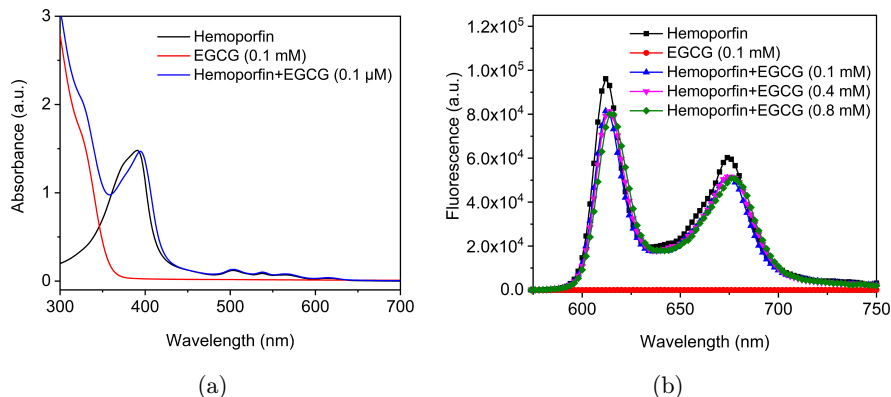


Fig. 2. Absorption spectra (a) and fluorescence spectra (b) of Hemoporphin, EGCG and Hemoporphin+EGCG. The concentrations of Hemoporphin for all measured samples are 20 μM.

luminescence curves and the corresponding integrated intensity are significantly decreased with the increase of EGCG concentrations (control, 0.2, 0.4, 0.6, 0.8 mM). Notably, the rising edge of ¹O₂ luminescence of the EGCG+Hemoporphin mixture shows a gradual blue shift in comparison with that of the pure Hemoporphin. In addition, the lifetimes of triplet-state Hemoporphin (τ_T) and ¹O₂ (τ_Δ) are indirectly derived by fitting the ¹O₂ luminescence curves in Fig. 3(a) using Eq. (2). The Stern–Volmer plots in the absence and presence of EGCG are presented in Fig. 3(b). According to the slope of the Stern–Volmer plot, the EGCG quenching rate constants for triplet-state Hemoporphin and ¹O₂ are determined to be $(6.8 \pm 0.4) \times 10^8 \text{ M}^{-1}\text{s}^{-1}$ and $(1.5 \pm 0.1) \times 10^8 \text{ M}^{-1}\text{s}^{-1}$, respectively. The quenching rate constant of ¹O₂ for Hemoporphin is comparable to the previously reported value of $(1.70 \pm 0.02) \times 10^8 \text{ M}^{-1}\text{s}^{-1}$ for Hiporfin.¹⁵

3.3. Dynamic monitoring of photodynamic-induced vascular damage during PDT

During PDT, the photodynamic damage to blood vessels in the DSWC model with various EGCG concentrations was dynamically monitored by NBI and LSCI. All images were captured every 15.0 s for a total period of 449.5 s, while an exposure time of 0.5 s was used for NBI. Dynamic changes of NBI, FI and LSCI of blood vessels in the DSWC model before and after PDT (i.e., total treatment time for 77.5 s) are shown in Fig. 4. For the EGCG group, no evident fluorescence was observed in blood vessels while the fluorescence intensity of group 2 was slightly higher than that of groups 3–7. Furthermore, all the arteries became invisible after PDT for group 2 in comparison with the veins, as indicated in the LSCI images in Fig. 4. For groups 3–7, the

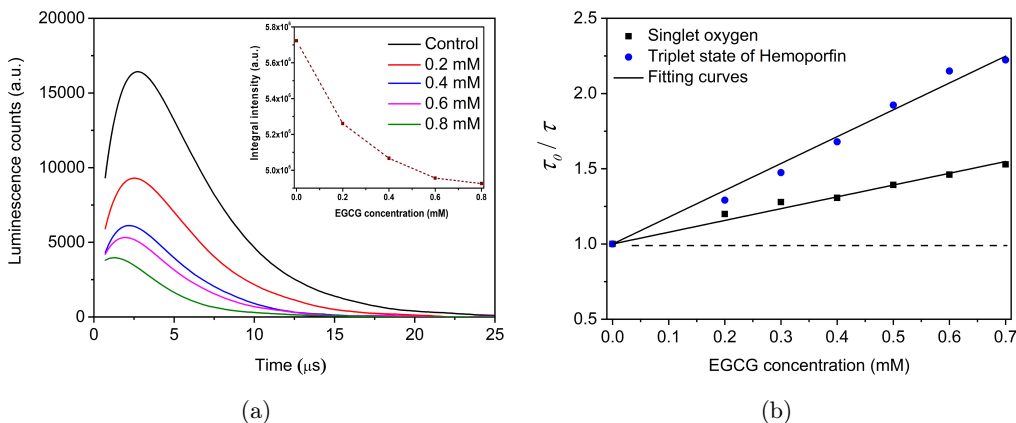


Fig. 3. Time-resolved ¹O₂ luminescence decay traces at 1270 nm of Hemoporphin with EGCG at various concentrations (Inset: the integrated intensity of ¹O₂ luminescence versus the EGCG concentration) (a). Ratios of lifetimes of triplet-state Hemoporphin and ¹O₂ versus the EGCG concentration, and τ_0 and τ refer to the lifetimes in the absence and presence of EGCG (b).

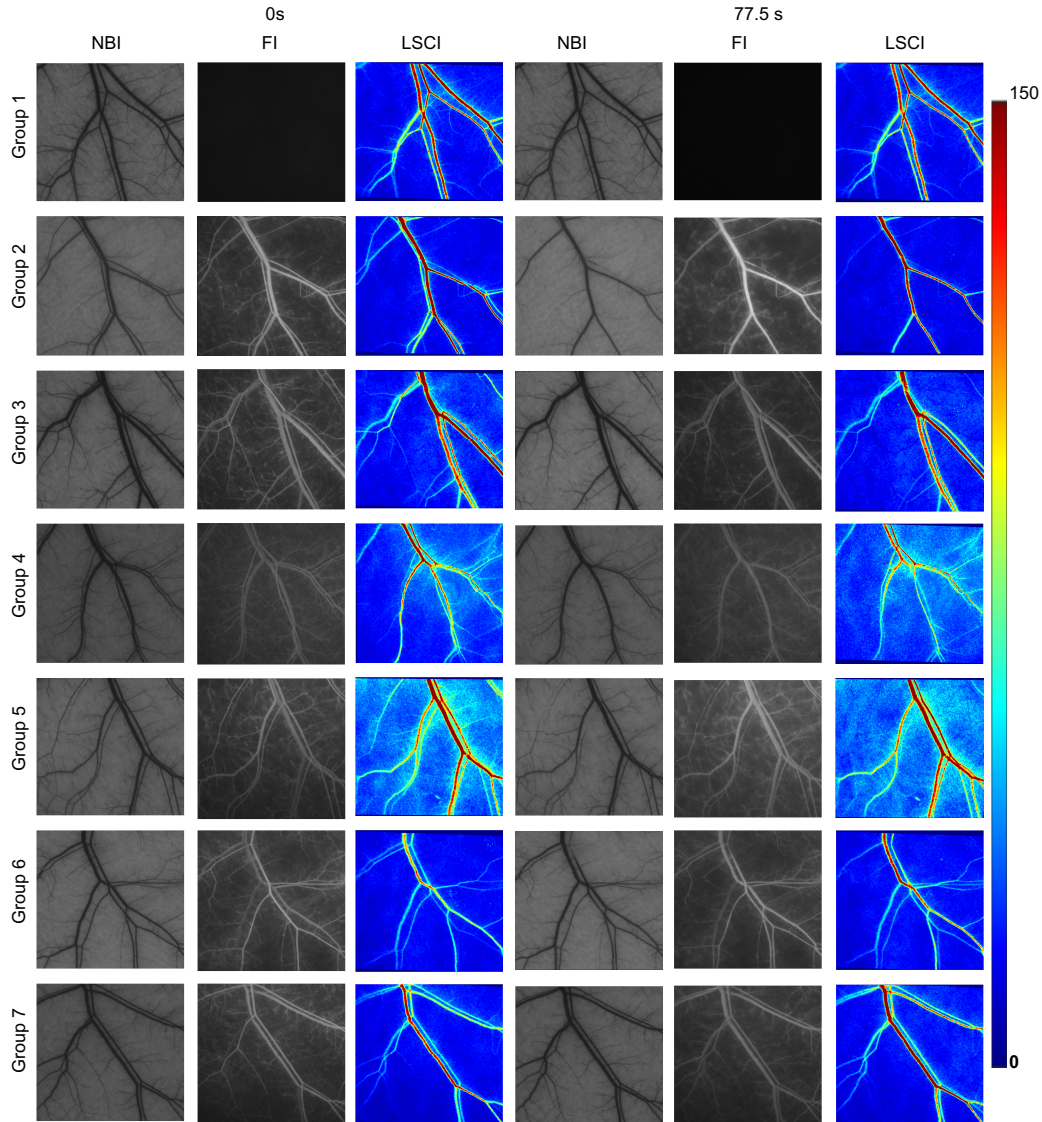


Fig. 4. Dynamic changes of NBI, FI and LSCI of blood vessels in the DSWC model before and after PDT ($n = 3$). The color bar and color scale applied to LSCI images show the relative blood flow values.

blood flow in arteries remained observable even when the arteries and veins were partially constricted.

To evaluate the regulation ability of EGCG for photodynamic damage of blood vessels, eight random ROI images of arteries and veins in the DSWC model were manually extracted from Fig. 4. The vasoconstriction was quantified with Eq. (3) and the vasoconstriction of arteries and veins versus treatment time during PDT were plotted in Fig. 5.

As illustrated in Fig. 5(a), slight constriction was observed for both arteries and veins for group 1. It is obvious that the arteries of group 2 were fully constricted after PDT for 77.5 s, while the arteries

began to recover from the constriction when the treatment time was 217.0 s, as indicated in Fig. 5 (b). In contrast to the arteries, the veins were gradually constricted with increasing treatment time, and no vascular recovery was found in the following observation. In this case, the vasoconstrictions of arteries and veins were determined to be $87.93 \pm 19.11\%$ and $44.02 \pm 5.95\%$, respectively.

In contrast with Figs. 5(a) and 5(b), the regulation ability of EGCG for Hemoporphin-mediated PDT could be clearly seen from Fig. 5(c) to Fig. 5 (g), which show less vasoconstriction in groups 3–7 than that of group 2 after PDT. As shown in Fig. 5(h), significant differences in arterial

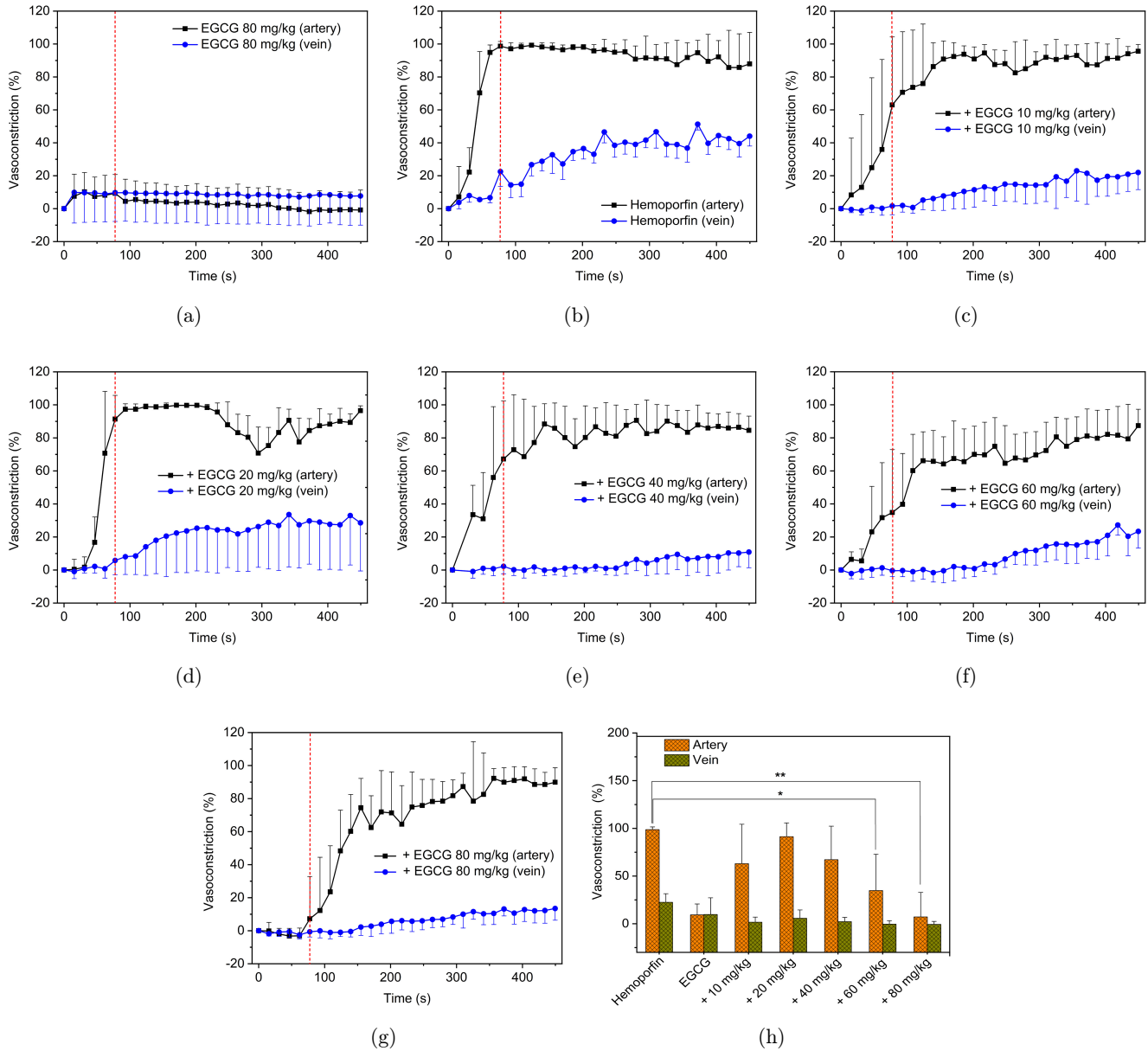


Fig. 5. Vasoconstriction of arteries and veins in DSWC model versus treatment time after PDT treated with (a) group 1, (b) group 2, (c) group 3, (d) group 4, (e) group 5, (f) group 6 and (g) group 7. (h) Vasoconstriction of arteries and veins in DSWC model after PDT with the light dose of 3.875 J/cm^2 .

vasoconstriction among group 2, group 6 ($*p < 0.05$) and group 7 ($**p < 0.01$) were observed.

To further confirm the potential of EGCG for healthy tissue protection, hydrogels with various EGCG concentrations were topically applied on blood vessels in the DSWC model 1.0 h before Hemoporfin-mediated PDT. As shown in Fig. 6, the DSWC model was divided into the regions of control and protection areas by various EGCG-containing hydrogels for comparison during

PDT, and the smooth blood circulation was observed after PDT for blood vessels pre-treated by the hydrogel with EGCG.

As illustrated in Fig. 7, the vasoconstriction of arteries and veins for both the control region with hydrogel alone and the protected region with EGCG hydrogel in the same DSWC model were quantitatively analyzed. Vasoconstrictions of arteries and veins after PDT for 77.5 s are listed in Table 3. In general, blood vessels in the protected

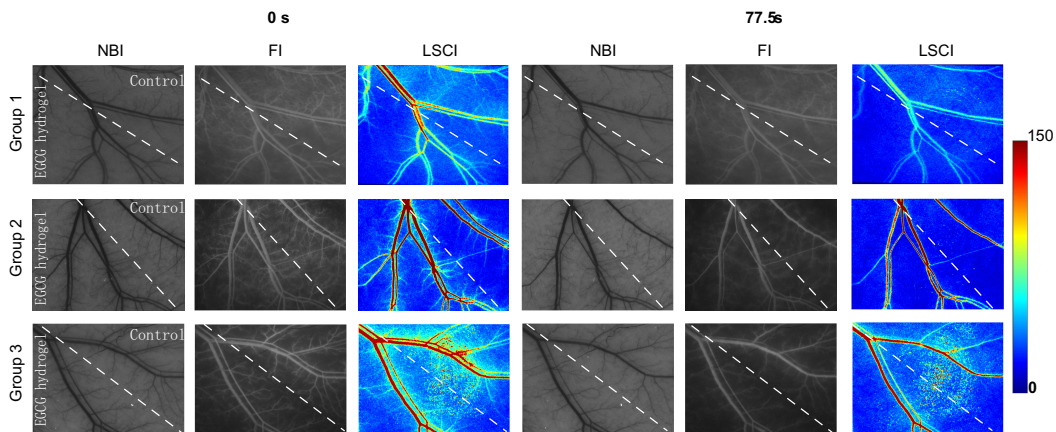


Fig. 6. Dynamic changes of the NBI, FI and LSCI of blood vessels in the DSWC model after topically applied hydrogel in the absence and presence of EGCG during PDT. The color bar and color scale applied to LSCI images show the relative blood flow values.

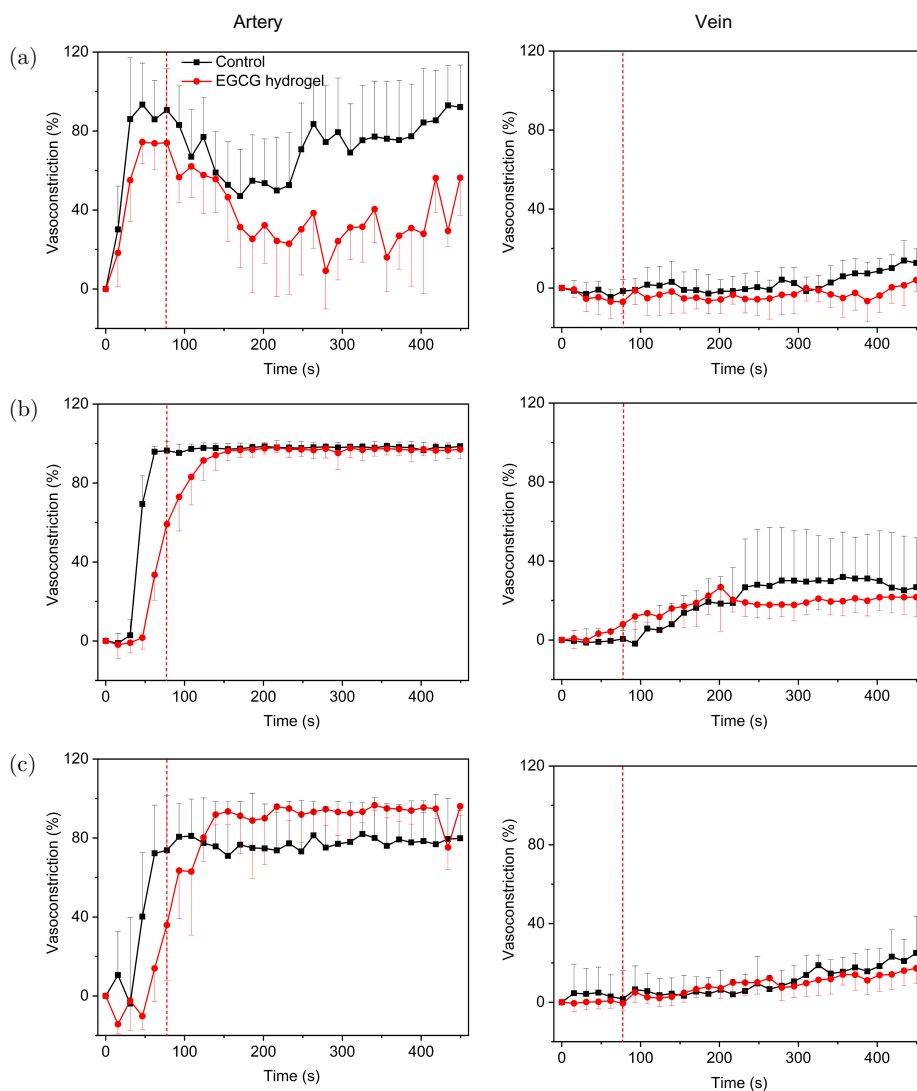


Fig. 7. Vasoconstriction of arteries and veins treated with hydrogels in the absence and presence of (a) 10 mg/mL, (b) 20 mg/mL and (c) 30 mg/mL EGCG in the same DSWC model.

Table 3. Vasoconstriction of arteries and veins for both the control region with hydrogel alone and the protected region with EGCG-containing hydrogel after PDT for 77.5 s.

Group	Region	Vasoconstriction (%)	
		Arteries	Veins
1	Control	90.60	-1.57
	EGCG hydrogel	74.00	-6.99
2	Control	98.42	0.56
	EGCG hydrogel	59.13	7.96
3	Control	73.93	1.71
	EGCG hydrogel	35.93	-0.52

region with EGCG hydrogel show less vasoconstriction than that of the control region with hydrogel alone.

4. Discussion

The fluorescence intensity of Hemoporphin in PBS was decreased by the additional EGCG. A possible explanation for this is that the Hemoporphin fluorescence was quenched by EGCG based on energy transfer between Hemoporphin at the excited state and EGCG molecules, which is similar to supposition in the previous study.²⁵ As illustrated in Fig. 8, both the fluorescence spectrum and the time-resolved NIR luminescence decay traces could be quenched by EGCG. The EGCG in arteries and vein might directly quench fluorescence, triplet-state Hemoporphin and $^1\text{O}_2$ luminescence through photodynamic processes, and thus reduce the

quantum yield of $^1\text{O}_2$ production.¹⁵ It can be assumed that the vasoconstriction of arteries and veins may be regulated through control of $^1\text{O}_2$ generation by EGCG. In contrast with groups 3–7, the higher fluorescence intensity of group 2 could be explained by the quenching effect of EGCG on Hemoporphin fluorescence. More importantly, the observable blood flow in arteries implied that EGCG could effectively reduce the PDT-induced damage to blood vessels.

In Fig. 5(a), the slight vascular constriction for group 1 could be attributed to the hyperthermia from laser irradiation during PDT. As shown in Fig. 5, the antioxidative effect of EGCG for arteries was more obvious than that of veins, which could be explained by the richer elastic fibers in arteries allowing higher elasticity.²⁶ In addition, the difference of platelet aggregation between arteries and veins induces the differences in EGCG-regulated vasoconstriction.²⁷ The highest vasoconstriction was achieved by group 4, implying that an appropriate EGCG concentration could increase vascular constriction through angiogenesis inhibition.²⁸ For this, the photodynamic damage of blood vessels for PDT is reduced by EGCG in a dose-dependent regulatory strategy. This finding agrees well with the previous observations by Sekowski *et al.* They demonstrated that UVB irradiation of bovine serum albumin induced S-S disruption and SH-group formation, which could be prevented by EGCG in a dose-dependent manner.²⁹ Therefore, the EGCG concentration needs to be optimized to maximally prevent PDT-induced oxidative damages to blood vessels.

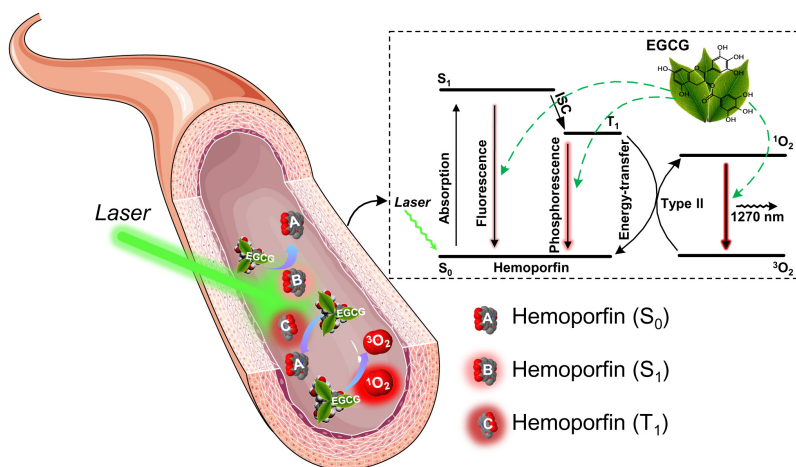


Fig. 8. Energy level diagram for $^1\text{O}_2$ generation and EGCG quenching processes in blood vessels (S_0 , S_1 and T_1 stand for ground state, singlet state and triplet PS, respectively).

For the experimental studies involving hydrogels, smooth blood circulation was observed after PDT for blood vessels pre-treated by the hydrogel with EGCG, suggesting that the PDT-induced oxidative damage to blood vessels could be effectively reduced by the permeation of EGCG hydrogel. In addition, significantly different vasoconstrictions of blood vessels pre-treated by the hydrogel alone and by the EGCG-containing hydrogel were apparently detected, as expected.

As illustrated in Table 3, the arteries pre-treated with hydrogel alone were more rapidly constricted than that of the arteries pre-treated with EGCG hydrogel with the increasing PDT treatment time. Moreover, vasoconstrictions of veins in the region with EGCG hydrogel were lower than that of arteries, which is in good accordance with the previous observation in Fig. 5. Due to the higher oxygen content in arteries, the arteries have a faster response in the early stages of treatment, as compared to the veins. Consequently, EGCG possesses a greater impact on the arteries with the increase of its concentration. In particular, the arteries in group 3 demonstrate a lower vasoconstriction as compared to groups 1 and 2, and a slower shrinkage rate was achieved with the increasing EGCG concentration, as expected. In addition, the arteries in the EGCG-protected region of group 3 indicate more obvious vascular constriction after PDT for 77.5 s, as compared to the control region. One reason may be that the intervention of EGCG reduces oxygen consumption, thereby enhancing the therapeutic efficiency of PDT.³⁰ For this, it should be noted that the optimal protocol for the use of EGCG needs to be further explored for clinical PDT application.

5. Conclusions

The EGCG quenching rate constants for triplet-state Hemoporphin and photosensitization-generated $^1\text{O}_2$ are determined to be $6.8 \times 10^8 \text{ M}^{-1}\text{S}^{-1}$ and $1.5 \times 10^8 \text{ M}^{-1}\text{S}^{-1}$, respectively. The vasoconstriction of blood vessels in the protected region with EGCG-containing hydrogel is lower than that of the control region with hydrogel alone after Hemoporphin-mediated PDT, suggesting that the photodamage of Hemoporphin could be efficiently reduced with EGCG for blood vessels of the protected region. This study demonstrates that EGCG is an efficient quencher for triplet-state Hemoporphin and $^1\text{O}_2$, and EGCG could be potentially used to reduce the undesired

photodamage of normal tissue in clinical PDT. However, the practical applications of EGCG are limited by several factors, including temperature, light, pH and oxygen, which may significantly accelerate its decomposition. Although conjugating EGCG with gel has the potential to retard its degradation, accurately determining the concentration of EGCG that penetrates in real scenarios remains challenging. In order to achieve the optimal regulatory function realization, it is crucial to optimize the concentration of EGCG through quantification of ROS level during PDT in future studies.


Acknowledgments

This work was supported by the National Natural Science Foundation of China (Grant Nos. 61935004, 62227823 and 61805040) and the Beijing Institute of Technology Research Fund Program for Young Scholars (XSQD-202123001).


Conflict of Interest


The authors have no conflicts of interest relevant to this paper.


ORCID


Tianlong Chen  <https://orcid.org/0009-0008-2001-1950>


Yi Shen  <https://orcid.org/0000-0003-4841-7561>

Li Lin  <https://orcid.org/0009-0009-3341-1387>

Huiyun Lin  <https://orcid.org/0009-0004-3608-1866>

Xuejiao Song  <https://orcid.org/0000-0002-5833-7381>

Defu Chen  <https://orcid.org/0000-0002-7198-1104>

Buhong Li  <https://orcid.org/0000-0001-9762-9187>

References

1. F. Borgia, R. Giuffrida, E. Caradonna, M. Vaccaro, F. Guarneri, S. P. Cannavò, "Early and late onset side effects of photodynamic therapy," *Biomedicines* **6**, 12 (2018).
2. U. Chilakamarthi, L. Giribabu, "Photodynamic therapy: Past, present and future," *Chem. Rec.* **17**, 775–802 (2017).

3. X. Liang, M. Mu, B. Chen, D. Chuan, N. Zhao, R. Fan, X. Tang, H. Chen, B. Han, G. Guo, "BSA-assisted synthesis of nanoreactors with dual pH and glutathione responses for ferroptosis and photodynamic synergistic therapy of colorectal cancer," *Mater. Today Adv.* **16**, 100308 (2022).
4. D. Chuan, H. Hou, Y. Wang, M. Mu, J. Li, Y. Ren, N. Zhao, B. Han, H. Chen, G. Guo, "Multifunctional metal-polyphenol nanocomposite for melanoma targeted photo/chemodynamic synergistic therapy," *J. Mater. Sci. Technol.* **152**, 159–168 (2023).
5. X. Chen, Z. Yi, G. Chen, X. Ma, Q. Tong, L. Tang, X. Li, "Engineered fabrication of EGCG-UV absorber conjugated nano-assemblies for antioxidative sunscreens with broad-band absorption," *Colloids Surf. B Biointerfaces.* **220**, 112912 (2022).
6. Q. Tong, Y. Xiao, Z. Yi, X. Chen, X. Jiang, X. Li, "Polyphenolic condensation assembly enabled biocompatible, antioxidative and light-colored tea sunscreen formulations with broadband UV protection," *Green Chem.* **25**, 4387–4041 (2023).
7. R. Y. Gan, H. B. Li, Z. Q. Sui, H. Corke, "Absorption, metabolism, anti-cancer effect and molecular targets of epigallocatechin gallate (EGCG): An updated review," *Crit. Rev. Food Sci. Nutr.* **58**, 924–941 (2018).
8. J. W. Gu, K. L. Makey, K. B. Tucker, E. Chinchar, X. Mao, I. Pei, E. Y. Thomas, L. Miele, "EGCG, a major green tea catechin suppresses breast tumor angiogenesis and growth via inhibiting the activation of HIF-1 α and NF κ B, and VEGF expression," *Vasc. Cell* **5**, 9 (2013).
9. A. Ferrario, M. Luna, N. Rucker, S. Wong, C. J. Gomer, "Pro-apoptotic and anti-inflammatory properties of the green tea constituent epigallocatechin gallate increase photodynamic therapy responsiveness," *Lasers Surg. Med.* **43**, 644–650 (2011).
10. S. T. Mun, D. H. Bae, W. S. Ahn, "Epigallocatechin gallate with photodynamic therapy enhances antitumor effects *in vivo* and *in vitro*," *Photodiagnosis Photodyn. Ther.* **11**, 141–147 (2014).
11. H. Qi, N. Abe, B. Zhu, Y. Murata, Y. Nakamura, "(–)-Epigallocatechin-3-gallate ameliorates photodynamic therapy responses in an *in vitro* T lymphocyte model," *Phytother. Res.* **28**, 1486–1491 (2014).
12. C. Hu, F. Zhang, Q. Kong, Y. Lu, B. Zhang, C. Wu, R. Luo, Y. Wang, "Synergistic chemical and photodynamic antimicrobial therapy for enhanced wound healing mediated by multifunctional light-responsive nanoparticles," *Biomacromolecules* **20**, 4581–4592 (2019).
13. D. S. Choi, M. Y. Jung, "Protective activities of catechins on singlet oxygen induced photooxidation of α -terpinene in methanol: Structure and singlet oxygen quenching activity relationship," *Food Sci. Biotechnol.* **22**, 249–256 (2013).
14. Y. Okazaki, Y. Ishidzu, F. Ito, H. Tanaka, M. Hori, S. Toyokuni, "L-Dehydroascorbate efficiently degrades non-thermal plasma-induced hydrogen peroxide," *Arch. Biochem. Biophys.* **700**, 08762 (2021).
15. X. Liao, C. Yang, H. Lin, B. Li, "Quenching effects of (–)-Epigallocatechin gallate for singlet oxygen production and its protection against oxidative damage induced by Ce6-mediated photodynamic therapy *in vitro*," *Photodiagnosis Photodyn. Ther.* **36**, 102467 (2021).
16. M. Yang, X. Li, G. Kim, R. Wang, S. J. Hong, C. H. Lee, J. Yoon, "A J-aggregated nanoporphyrin overcoming phototoxic side effects in superior phototherapy with two-pronged effects," *Chem. Sci.* **13**, 12738–12746 (2022).
17. B. Li, L. Lin, Enhanced photodynamic therapy, *Biomedical Photonic Technologies*, Z. Zhang, S. Jiang, B. Li, Eds., pp. 165–199, Wiley-VCH GmbH, Weinheim (2023).
18. B. Yuan, Y. Cao, Q. Tang, Z. Yuan, Y. Zhou, J. M. David, C. Cao, "Enhanced performance and functionality of active edible films by incorporating tea polyphenols into thin calcium alginate hydrogels," *Food Hydrocolloids* **97**, 105197 (2019).
19. B. S. Kim, S. H. Kim, K. Kim, Y. H. An, K. H. So, B. G. Kim, N. S. Hwang, "Enzyme-mediated one-pot synthesis of hydrogel with the polyphenol cross-linker for skin regeneration," *Mater. Today Bio.* **8**, 100079 (2020).
20. L. Lin, H. Lin, Y. Shen, D. Chen, Y. Gu, B. C. Wilson, B. Li, "Singlet oxygen luminescence image in blood vessels during vascular targeted photodynamic therapy," *Photochem. Photobiol.* **96**, 646–651 (2020).
21. B. Liu, Z. Kang, W. Yan, "Synthesis, stability, and antidiabetic activity evaluation of (–)-Epigallocatechin Gallate (EGCG) palmitate derived from natural tea polyphenols," *Molecules* **26**, 393 (2021).
22. Y. Shen, F. Liang, Y. Niu, H. Lin, Y. Gu, B. C. Wilson, B. Li, "Monitoring vascular targeted PDT response with multimode optical imaging," *Proc. SPIE* **10879**, 1087906 (2019).
23. X. Xu, L. Lin, B. Li, "Automatic protocol for quantifying the vasoconstriction in blood vessel image," *Biomed. Opt. Exp.* **11**, 2122–2136 (2020).
24. X. Xu, Y. Shen, L. Lin, L. Lin, B. Li, "Multi-step deep neural network for identifying subfascial

- vessels in a dorsal skinfold window chamber model,” *Biomed. Opt. Exp.* **13**, 426–437 (2021).
25. M. Kou, F. Qin, W. Lu, Z. Hu, Z. Zhang, “A new insight into the singlet oxygen mechanism for photodynamic therapy,” *J. Phys. Chem. Lett.* **14**, 5613–5617 (2023).
 26. L. Niklason, G. Dai, “Arterial venous differentiation for vascular bioengineering,” *Annu. Rev. Biomed. Eng.* **20**, 431–447 (2018).
 27. B. C. Cooley, “*In vivo* fluorescence imaging of large-vessel thrombosis in mice,” *Arterioscler. Thromb. Vasc. Biol.* **31**, 1351–1356 (2011).
 28. C. Y. Chen, Y. J. Lin, C. Y. H. Wang, S. J. Lan, M. J. Sheu, “Epigallocatechin-3-gallate inhibits tumor angiogenesis: Involvement of endoglin/Smad1 signaling in human umbilical vein endothelium cells,” *Biomed. Pharmacother.* **120**, 109491 (2019).
 29. S. Sekowski, M. Terebka, A. Veiko, U. Sulkowska, I. B. Zavodnik, N. Abdulladjanova, S. Mavlyanov, A. Roszkowska, M. Zamaraeva, “Epigallocatechin gallate (EGCG) activity against UV light-induced photo damages in erythrocytes and serum albumin—Theoretical and experimental studies,” *J. Photochem. Photobiol. A Chem.* **356**, 379–388 (2018).
 30. X. S. Li, J. F. Lovell, J. Yoon, X. Y. Chen, “Clinical development and potential of photothermal and photodynamic therapies for cancer,” *Nat. Rev. Clin. Oncol.* **17**, 657–674 (2020).